

Monolayer Fe_3GaX_2 (X=I, Br, Sb): high-temperature two-dimensional magnets and a novel partially ordered spin state

Qiu hao Wang,^{1,2,3} Xinlong Yang,^{2,3} Fawei Zheng,^{2,3,*} and Ping Zhang^{1,4,†}

¹*School of Physics and Physical Engineering,
Qufu Normal University, Qufu 273165, China.*

²*Center for Quantum Physics, Key Laboratory of Advanced
Optoelectronic Quantum Architecture and Measurement (MOE),
School of Physics, Beijing Institute of Technology, Beijing 100081, China.*

³*Beijing Key Lab of Nanophotonics & Ultrafine Optoelectronic Systems,
School of Physics, Beijing Institute of Technology, Beijing 100081, China.*

⁴*Institute of Applied Physics and Computational Mathematics, Beijing 100088, China.*

Abstract

We systematically investigated the effects of charge doping and strain on monolayer Fe_3GaTe_2 , and proposed three new novel two-dimensional magnetic materials: monolayer Fe_3GaX_2 (X=I, Br, Sb). We found that both strain and charge doping can tune the magnetic interactions, and the tuning by charge doping is more significant. Differential charge analysis revealed that the doped charges predominantly accumulate around Te atoms. Based on this insight, we introduced Fe_3GaI_2 , Fe_3GaBr_2 , and Fe_3GaSb_2 monolayers. The Fe_3GaI_2 and Fe_3GaBr_2 monolayers contain I and Br atoms rather than Te atoms, emulate electron-doped Fe_3GaTe_2 monolayer, resulting in notably high T_c values of 867 K and 844 K, respectively. In contrast, the Fe_3GaSb_2 monolayer mimics hole-doped Fe_3GaTe_2 monolayer, presents a mix of FM and antiferromagnetic interactions, manifesting a distinctive partially ordered magnetic state. Our study demonstrates that substitution atoms based on the charge-doping effect offer a promising approach for predicting new magnetic materials. The proposed Fe_3GaI_2 , Fe_3GaBr_2 , and Fe_3GaSb_2 monolayers hold great potential for spintronics applications, and may stimulate the pursuit of new types of spin liquid.

* Corresponding author: fwzheng@bit.edu.cn

† Corresponding author: zhang_ping@iapcm.ac.cn

In 2017, researchers reported two-dimensional (2D) materials with long-range ferromagnetic order[1, 2]. Since then, 2D magnets have attracted great attention because of their diverse physical properties and potential device applications. For example, combining a 2D magnet and 2D superconductor might produce a topological superconductor[3] that can be used to construct a quantum computer. Combining two monolayer CrI₃ magnets leads to a bilayer CrI₃, which has stacking-dependent interlayer spin exchange interactions[4] that change the magnetic state from antiferromagnetic (AFM) to ferromagnetic (FM) and produces giant tunneling magnetoresistance[5]. Furthermore, introducing a twist to the system can produce complex spin textures[6] and might support Skyrmions[7, 8], which can be used to construct memory devices and spin wave generators. These studies render 2D magnets promising materials for future nano-devices. However, these applications are limited by the Curie temperature (T_c) of 2D magnets. The T_c of monolayer CrI₃ is 45 K[1] and that of bilayer CrGeTe₃[2, 9] is even lower at only 28 K. Therefore, efforts have been made to increase the T_c of 2D magnets. Tuning methods, such as strain[10, 11] and charge doping[11, 12], can be used to increase the T_c of 2D magnets. The T_c of CrI₃ can be increased by about 10% under heavy charge doping[13], and increased by 36% under 10% stretch strain[14]. In theoretical calculations, the T_c of CrCl₃ and CrBr₃ is increased by 33% and 60%, respectively, under 10% stretch strain[14], and the T_c of CrGeTe₃ might increase by 45% under charge doping[15].

In addition to tuning currently available 2D magnets, new 2D magnets have been found. First, atomically thin Fe₃GeTe₂ exhibits intrinsic ferromagnetism, the T_c of which is up to 200 K[16, 17]. In addition, monolayer Fe₅GeTe₂ [18] exhibits $T_c = 270$ K. More examples can be found elsewhere[19, 20]. Nevertheless, 2D magnets with a T_c higher than room temperature remain rare. Recently, Fe₃GaTe₂ was reported[21] to have a T_c higher than 350 K. Its atomic structure is similar to that of Fe₃GeTe₂; the only difference is that the Ge atoms are replaced with Ga atoms. Further research[22–24] indicates an excellent magnetoresistance of spin-valve devices composed of Fe₃GaTe₂, which function well at 300 K under low current conditions. In addition, the exchange bias effect of Fe₃GaTe₂ nanoflakes has been revealed experimentally[25]. Even though many studies on Fe₃GaTe₂ have been reported, research on the fundamental properties of Fe₃GaTe₂ monolayers is still lacking.

In this work, on the basis of first-principles calculations and classical Monte Carlo simulations, we systematically studied the strain and charge doping effects of Fe₃GaTe₂ monolayers,

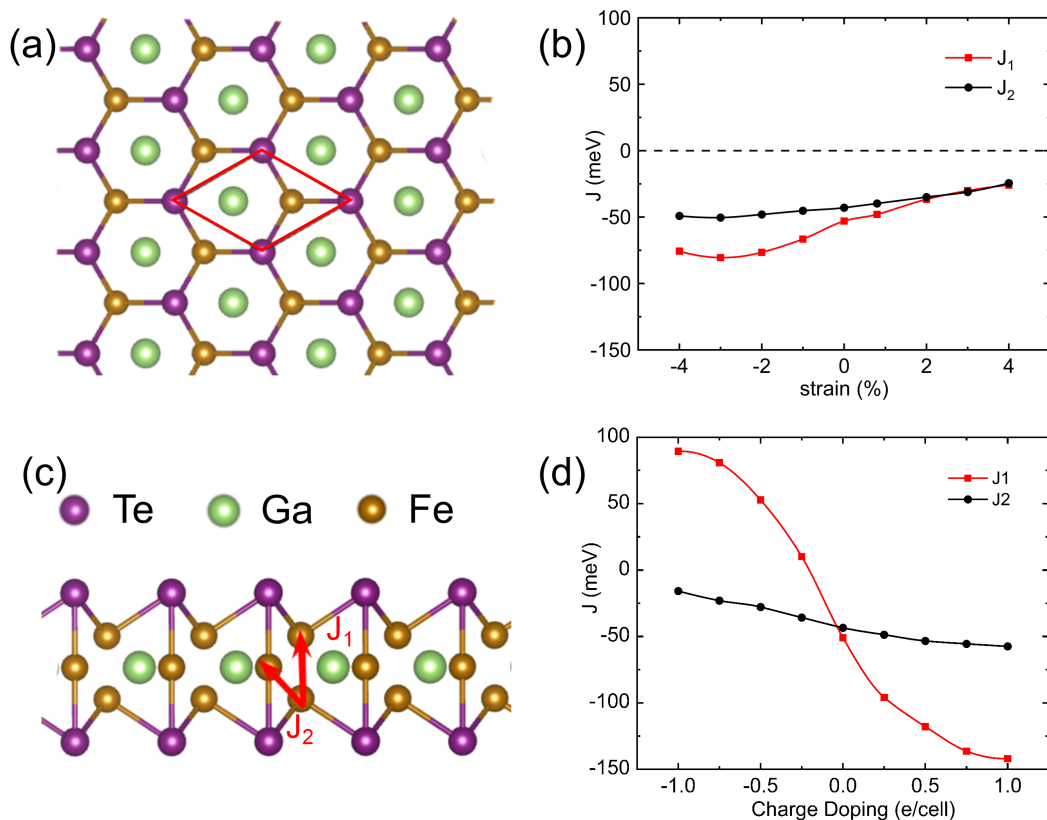


FIG. 1. The (a) top and (c) side views of an Fe₃GaTe₂ monolayer. The red rhombus in (a) indicates the primitive cell, and the two red arrows in (b) indicate the nearest and second-nearest neighboring spin exchange interactions. Values of the spin exchange constants under charge doping and biaxial strain are shown in (b) and (d), respectively.

and proposed three new 2D magnetic materials. We found that strain and charge doping are effective methods for tuning the T_c of Fe₃GaTe₂ monolayers. The electron doping and compressive strain would increase the value of the T_c . The T_c reaches 513 K under one electron doping per unit cell, and it is above 400 K under 2% compressive strain. Conversely, hole doping and extensile strain weaken the spin exchange interactions, and hence decrease the T_c . On the basis of the detailed analysis of the doping charge distributions, we propose Fe₃GaI₂, Fe₃GaBr₂, and Fe₃GaSb₂ monolayer. Fe₃GaI₂ and Fe₃GaBr₂ have high T_c , and Fe₃GaSb₂ has a unique magnetic state that is partially ordered.

We performed all density functional theory calculations with the Vienna ab initio simulation package[26, 27]. To increase calculation efficiency, we used the projector augmented wave (PAW) method[28] to describe the core electrons. The exchange-correlation function

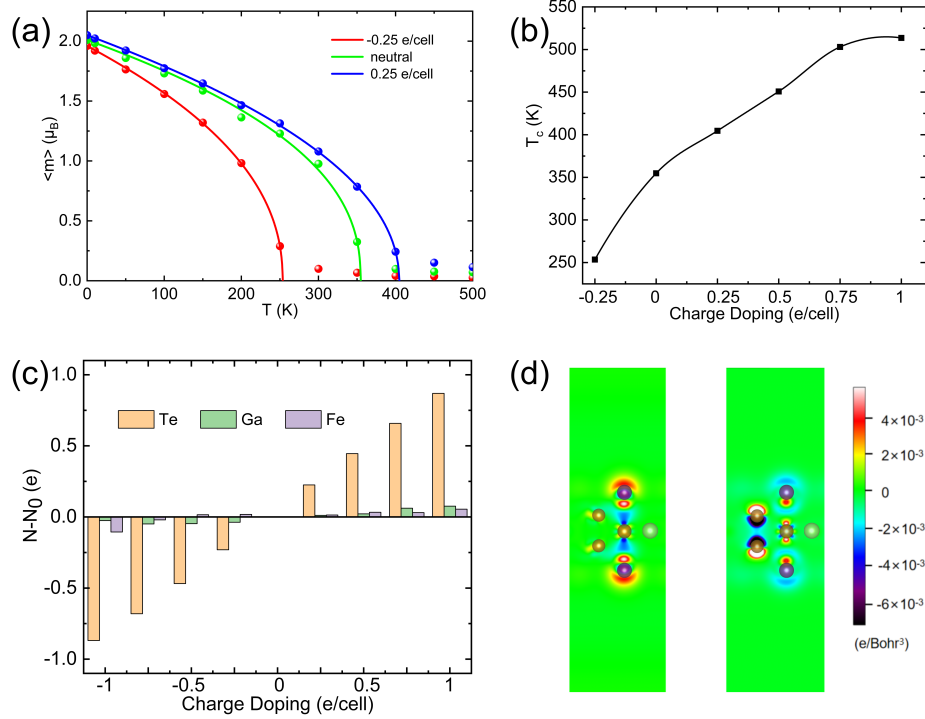


FIG. 2. (a) The magnetic polarizations as functions of temperature obtained by performing Monte Carlo simulations. (b) The curve for T_c under various doping levels. (c) Doping charge accumulation for each element, obtained by using Bader's analysis. (d) Differential charge density for the 0.5-electron-doped (left panel) and 0.5-hole-doped (right panel) Fe_3GaTe_2 monolayer.

was approximated using the generalized gradient approximation (GGA) parameterized by Perdew, Burke, and Ernzerhof (PBE)[29]. The plane wave cutoff energy was set to 400 eV. Brillouin zone integrations were conducted on a $12 \times 12 \times 1$ Gamma-centered K-point mesh. A vacuum of 20 Å was employed to prevent interactions between periodic images. The cutoff energy, K-point mesh, and vacuum space were all optimized in our test calculations. The atomic structures were optimized until the force on each atom was less than 0.001 eV/Å. Phonon dispersions were determined using the Phonopy package, where the real space force constants were obtained based on a $3 \times 3 \times 1$ supercell and density functional perturbation theory (DFPT)[30] as implemented in VASP. To obtain the value of T_c , the heat bath Monte Carlo method[31] was employed. The simulations were performed on a $90 \times 90 \times 1$ supercell with 150,000 simulation steps.

The Figure 1a,c show the atomic structure of the Fe_3GaTe_2 monolayer. It consists of five layers of atoms. The top and bottom outermost layers consist of Te atoms, whereas

the central layer consists of Ga and Fe atoms. The other two layers are all composed of Fe atoms. The magnetic moments of these Fe atoms differ. The magnetic moment of a Fe atom at the central layer is $1.4 \mu_B$, whereas that of a Fe atom at the other layers is $2.3 \mu_B$. All the Fe atoms form a hexagonal structure in the top view, and the Ga atoms are located at the centers of the hexagons. The relaxed lattice parameter is $a=3.99\text{\AA}$, which is close to the experiment value[21].

The Fe_3GaTe_2 monolayer contains three layers of magnetic atoms; therefore, there are many different spin exchange interactions. The Hamiltonian of this system as,

$$H = \sum_{ij} J_{ij} \mathbf{S}_i \cdot \mathbf{S}_j \approx J_1 \sum_{1nn} \mathbf{S}_i \cdot \mathbf{S}_j + J_2 \sum_{2nn} \mathbf{S}_i \cdot \mathbf{S}_j$$

where the \mathbf{S}_i and \mathbf{S}_j are spins at site i and j , and the constant J_{ij} describes the spin exchange interaction between them. A previous study[21] calculated these interactions up to the seventh nearest neighbors. The most important interactions are the first and second nearest neighboring interactions, as indicated in Figure 1a with J_1 and J_2 . All the other interactions are much smaller than them. We checked (by performing Monte Carlo simulations) that the value of T_c is determined by J_1 and J_2 . The contribution from the other interactions is negligible. We obtained the values of J_1 and J_2 by using the four-state method[32]. These values are -51.0 meV and -43.4 meV in our calculations, leading to $T_c = 355$ K, which agrees well with the experimental results[21].

Firstly, we consider the strain effect of the Fe_3GaTe_2 monolayer. We applied biaxial strain in the range of $-4\% \sim 4\%$. Figure 1b shows the calculated values of J_1 and J_2 . The extensile strain monotonously weakens both J_1 and J_2 . However, the compressive strain in the range of $0 \sim -3\%$ enhances J_1 and J_2 , thus increases the value of T_c . The values of J_1 and J_2 are -76.6 meV and -48.1 meV under -2% compressive strain. The corresponding T_c is above 400 K, which suggests that the strain is an effective method of enhancing T_c . Nevertheless, a compressive strain larger than -3% weakens the J_1 interaction. Another commonly used tuning method for 2D materials is charge doping. We thus studied the charge doping effect of the Fe_3GaTe_2 monolayer. The maximum doping charge density is 1.0 e/cell for electron doping, and -1.0 e/cell for hole doping. Figure 1c shows the calculated spin exchange constants. In the case of electron doping, the two FM interactions are enhanced. At 1.0 e/cell, the value of J_1 increases by 176%, and that of J_2 increases by 32%. In contrast, hole doping weakens the two FM interactions. The J_1 changes sign at a doping density of -0.2

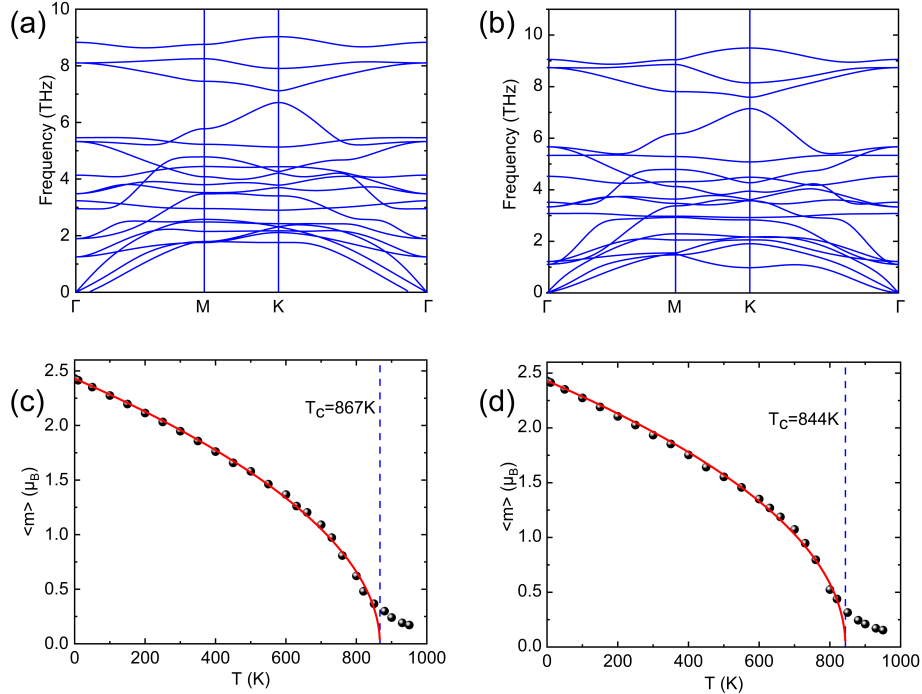


FIG. 3. The phonon dispersions of (a) Fe₃GaI₂ and (b) Fe₃GaBr₂ monolayers. Their magnetic polarizations as functions of temperature are shown in (c) and (d), respectively.

$e/cell$, and becomes an AFM interaction at heavier hole doping. Compared with the strain effect, the charge doping effect changes the J_1 and J_2 more substantially, rendering it a more effective means of tuning the magnetic properties of the Fe₃GaTe₂ monolayer.

We also calculated the tuning of T_c under charge doping. Figure 2a shows the simulated mean moments as functions of temperature. We calculated the values of T_c by fitting these data with $\langle m \rangle = m_0(1 - T/T_c)^\beta$, where $m_0 = 1$ for our Hamiltonian with normalized spins. The fitting result indicates that the T_c without charge doping is 355 K. The T_c increases to 404 K at 0.25 $e/cell$ electron doping, and decreases to 253 K at $-0.25 e/cell$ hole doping. At $-0.25 e/cell$ hole doping, J_1 has a small positive value, indicative of a weak AFM interaction. However, J_2 has a large negative value, which dominates the magnetic properties of the system. Thus, the system is still a FM, and the T_c is decreased by 30%.

To obtain the doping charge distribution, we performed Bader's analysis calculations[33]. We used the charge on each element after doping minus that of the neutral case to indicate the distribution of the doping charge. Figure 2c shows the calculation results, in which the charge on an element is the summation of the doping charges on all the atoms of the

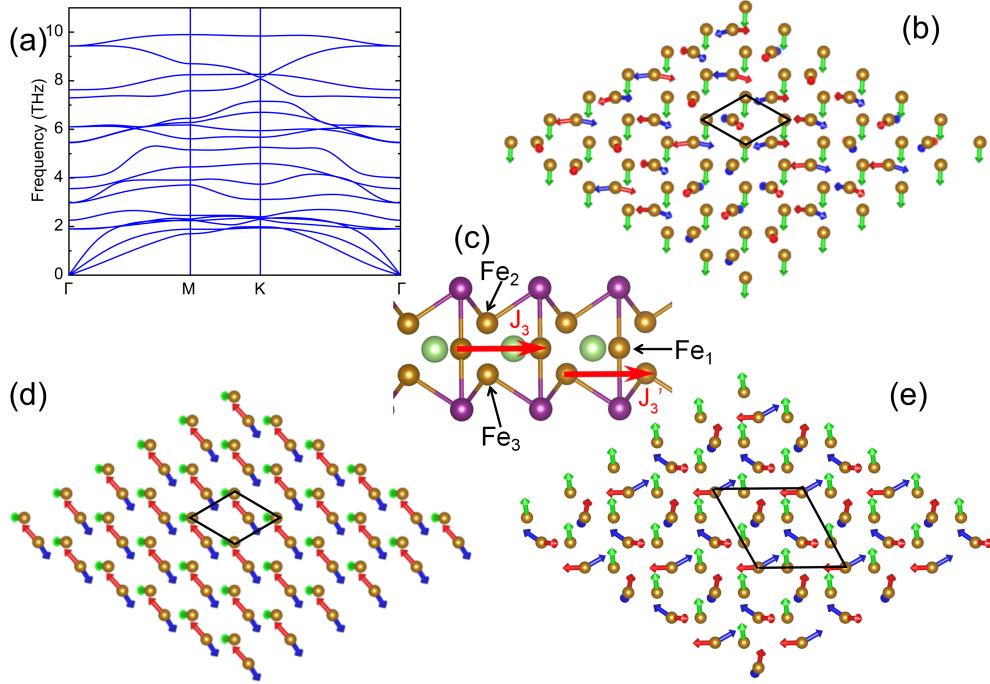


FIG. 4. (a) Phonon dispersions of Fe_3GaSb_2 monolayer. (b) Partially ordered ground magnetic state of Fe_3GaSb_2 monolayer. (c) Red arrows indicate the third nearest neighboring spin exchange interactions J_3 and J_3' . (d) Ground state after considering the weak interactions J_3 and J_3' . (e) Ground state of Fe_3GaSb_2 monolayer under 2% extensile strain.

element in a unit cell. A large quantity of the doping charges is located at the Te atoms. When the doping is 1 e/cell, the Te atoms absorb 85% of the total doping electrons. Further calculations indicate that this ratio is independent of the doping level. This conclusion is also confirmed by the calculation of differential charge density as shown in Figure 2d, which is defined as the difference of charge density after and before doping. The differential charge density around the Ga atom is small, which explains the small doping charges in Bader's analysis. The differential charge density on the central Fe atom differs from that of the other two Fe atoms. Their values cancel, leaving a small doping charge on the Fe element. The most doping charges are around the Te atoms, located at the outside of the surface Te atoms. Almost all the doping charges are absorbed by the Te atoms, and therefore it is natural to simulate the heavy charge doping by substituting Te with other elements. For example, I and Br have one more valence electron than Te, and thus substituting Te would simulate heavy electron doping. Sb has one less valence electron than Te and thus can be used to simulate heavy hole doping.

After substituting Te atoms with I and Br atoms, two new materials are obtained: Fe_3GaI_2 and Fe_3GaBr_2 monolayers. Their lattice parameters are 4.13 and 4.10 Å which are slightly larger than that of the Fe_3GaTe_2 monolayer. We checked their stabilities by the phonon dispersions. The Figure 3a,b show the calculated phonon dispersions based on density functional perturbation theory, which clearly indicate that they are stable. First-principles molecular dynamics simulations also confirm that Fe_3GaI_2 and Fe_3GaBr_2 monolayers are stable at room temperature. In monolayer Fe_3GaI_2 and Fe_3GaBr_2 , the magnetic moment of the Fe atoms at the central layer are $2.1 \mu_B$, and those of the other layers are $2.6 \mu_B$. They are larger than that in the Fe_3GaTe_2 monolayer. By using the four-state method, we obtained the spin exchange constants of Fe_3GaI_2 and Fe_3GaBr_2 monolayers. The value of J_1 for the Fe_3GaI_2 monolayer is -196.8 meV, which is about 3 times larger than that of the Fe_3GaTe_2 monolayer. The value of J_2 is -97.4 meV. This is almost 2.2 times of the value in the Fe_3GaTe_2 monolayer. The values for the Fe_3GaBr_2 monolayer are $J_1 = -170.3$ and $J_2 = -99.7$ meV. These values are slightly smaller than that of the Fe_3GaI_2 monolayer, but still much larger than that of the Fe_3GaTe_2 monolayer. These trends agree with the charge doping effect in the Fe_3GaTe_2 monolayer. These strong FM interactions lead to high phase transition temperatures. The Figure 3c,d show the calculated curves of magnetization. The fitted transition temperatures are $T_c = 867$ K for the Fe_3GaI_2 monolayer and $T_c = 844$ K for the Fe_3GaBr_2 monolayer. They are much larger than room temperature, imparting these two materials with very stable FM states at room temperature.

Substitution of Te atoms in an Fe_3GaTe_2 monolayer with Sb atoms leads to a new material: an Fe_3GaSb_2 monolayer. An Sb atom has an approximately equal radius as a Te atom, and has one less valence electron. Thus, the substitution mimics the heavy hole doping of the Fe_3GaTe_2 monolayer. The phonon dispersions as shown in Figure 4a have no imaginary frequencies, suggesting that the system is stable. First-principles molecular dynamics simulations confirmed that the system is stable at room temperature. Details are in the Supporting Information. The magnetic moment of the central Fe atom (Fe_1) in the Fe_3GaSb_2 monolayer [Figure 4b] is $1.1 \mu_B$, and the magnetic moments for Fe_2 and Fe_3 are all $2.0 \mu_B$. These values are substantially smaller than that of the Fe atoms in the Fe_3GaTe_2 monolayer.

We calculated the spin exchange constants between these magnetic atoms. The value of J_1 for the Fe_3GaSb_2 monolayer is 78.2 meV, which is AFM rather than FM. The value of J_2

is -8.2 meV, which is FM but is much weaker than that of the neutral Fe_3GaTe_2 monolayer. Their trends are consistent with the hole doped Fe_3GaTe_2 monolayer as shown in Figure 1d. The strength of the AFM interaction described by J_1 is one order of magnitude larger than that of the FM interaction described by J_2 . Therefore, each pair of Fe_2 and Fe_3 atoms always has antiparallel magnetic moments (normalized moments are named as \mathbf{m}_2 and \mathbf{m}_3). For each pair of Fe_2 - Fe_3 , there are three nearest Fe_1 atoms. The couplings between Fe_1 and Fe_2 - Fe_3 are FM. Thus, the magnetic moments \mathbf{m}_2 and \mathbf{m}_3 are slightly tilted to the direction of the magnetic moment on Fe_1 (\mathbf{m}_1). Such tilting further polarizes the other two Fe_1 atoms. Thus, all the Fe_1 atoms have a parallel magnetic moment at the ground state. Suppose the Fe_1 atoms have all magnetic moment in x -direction, then the energy raised by a Fe_2 and Fe_3 can be written as:

$$\begin{aligned} E_{23} &= J_1 \mathbf{m}_2 \cdot \mathbf{m}_3 + 3J_2 \mathbf{m}_1 \cdot \mathbf{m}_3 + 3J_2 \mathbf{m}_1 \cdot \mathbf{m}_2 \\ &= \frac{1}{2} J_1 (\mathbf{m}_2 + \mathbf{m}_3)^2 + 3J_2 \mathbf{m}_1 \cdot (\mathbf{m}_2 + \mathbf{m}_3) + c. \end{aligned}$$

The first term is determined by the norm of $\mathbf{m}_2 + \mathbf{m}_3$, the second term is the projection of $\mathbf{m}_2 + \mathbf{m}_3$ to x -direction, and the last term is a constant $c = -J_1 \frac{m_2^2 + m_3^2}{2}$. Since the J_2 is negative, the minimum energy could be obtained by vary the direction of $\mathbf{m}_2 + \mathbf{m}_3$ to the x -direction, then the $E_{23} = \frac{1}{2} J_1 |\mathbf{m}_2 + \mathbf{m}_3|^2 + 3J_2 |\mathbf{m}_2 + \mathbf{m}_3| + c$. Then the $\mathbf{m}_2 + \mathbf{m}_3$ in the ground state can be obtained by $\frac{\partial E_{23}}{\partial |\mathbf{m}_2 + \mathbf{m}_3|} = 0$. The results show that the angle between \mathbf{m}_2 and \mathbf{m}_3 is 162° . We can see that the energy only depends on $\mathbf{m}_2 + \mathbf{m}_3$, thus it leaves the $\mathbf{m}_2 - \mathbf{m}_3$ an unstrained freedom. There should be infinite number of ground states in which each pair of Fe_2 - Fe_3 atoms have a randomly chosen direction of \mathbf{m}_2 - \mathbf{m}_3 . This analysis is confirmed by our Monte Carlo simulations, which provide the ground state as a peculiar partially ordered state, as shown in Figure 4b. Further weak interactions between Fe_2 - Fe_3 pairs might remove the randomness, and lead to a fully ordered ground state.

We then considered the third nearest interactions J_3 and J'_3 as shown in Figure 4c. The calculated J_3 is -2.7 meV and J'_3 is -0.6 meV. These FM interactions force the magnetic moments of Fe_2 - Fe_3 pairs to be distributed in an ordered manner as shown in Figure 4d. A small biaxial tensile strain (2%) can change the sign of J'_3 , which brings an ordered state in the $\sqrt{3} \times \sqrt{3}$ supercell as shown in Figure 4e. The value of J'_3 is 0.7 meV under biaxial tensile strain. Therefore, the Fe_3GaSb_2 monolayer has a complex ground magnetic state and is sensitive to the external biaxial tensile strain. The ordered states in Figure 4d,e might

be easily destroyed by small thermal or quantum fluctuations, and become partially ordered states again.

In conclusion, we used first-principles calculations and Monte Carlo simulations to investigate the magnetic interactions in Fe_3GaTe_2 monolayers under charge doping and biaxial strain, which leads to the propose of three novel 2D magnetic materials. Both the strain and charge doping can tune the magnetic interactions of the Fe_3GaTe_2 monolayer. A higher T_c can be obtained by electron doping or compressive strain, and the charge doping is more efficient than biaxial strain. The sign of J_1 can even be changed under heavy hole doping. By using the differential charge density and Bader's analysis, we reveal that the doped charge is mainly distributed around the Te atoms. Therefore, we propose three materials to mimic heavy electron doping and hole doping of Fe_3GaTe_2 monolayers: Fe_3GaI_2 , Fe_3GaBr_2 , and Fe_3GaSb_2 monolayers. I and Br atom substitution leads to Fe_3GaI_2 and Fe_3GaBr_2 monolayers, which are analogous to the heavy electron doped Fe_3GaTe_2 monolayer, have strong FM interactions, and lead to astonishingly high T_c . On the other hand, Sb atom substitution leads to an Fe_3GaSb_2 monolayer, which is analogous to the heavy hole doped Fe_3GaTe_2 monolayer. It has a unique partially ordered magnetic state. The model Hamiltonian and the special magnetic state inspires the possible existence of the partially ordered spin liquid. Our study provides an effective method to find new 2D magnetic materials; the proposed Fe_3GaI_2 and Fe_3GaBr_2 monolayers have potential applications in room-temperature spintronics, and the novel magnetic state of Fe_3GaSb_2 monolayer may stimulate the study of new spin liquids.

This work was supported by the National Natural Science Foundation of China under Grant Nos. 12022415, 12374054, and 11974056. We acknowledge the computing resources of the Tencent TEFS platform (<https://tefsccloud.com>).

-
- [1] Huang, B.; Clark, G.; Navarro-Moratalla, E.; Klein, D. R.; Cheng, R.; Seyler, K. L.; Zhong, D.; Schmidgall, E.; McGuire, M. A.; Cobden, D. H.; Yao, W.; Xiao, D.; Jarillo-Herrero, P.; Xu, X. Layer-dependent ferromagnetism in a van der Waals crystal down to the monolayer limit. *Nature* **2017**, *546*, 270–273.
- [2] Marti, X. et al. Room-temperature antiferromagnetic memory resistor. *Nature Materials* **2014**,

13, 367–374.

- [3] Kezilebieke, S.; Huda, M. N.; Vaño, V.; Aapro, M.; Ganguli, S. C.; Silveira, O. J.; Głodzik, S.; Foster, A. S.; Ojanen, T.; Liljeroth, P. Topological superconductivity in a van der Waals heterostructure. *Nature* **2020**, *588*, 424–428.
- [4] Sivadas, N.; Okamoto, S.; Xu, X.; Fennie, C. J.; Xiao, D. Stacking-Dependent Magnetism in Bilayer CrI₃. *Nano Letters* **2018**, *18*, 7658–7664.
- [5] Song, T.; Cai, X.; Tu, M. W.-Y.; Zhang, X.; Huang, B.; Wilson, N. P.; Seyler, K. L.; Zhu, L.; Taniguchi, T.; Watanabe, K.; McGuire, M. A.; Cobden, D. H.; Xiao, D.; Yao, W.; Xu, X. Giant tunneling magnetoresistance in spin-filter van der Waals heterostructures. *Science* **2018**, *360*, 1214–1218.
- [6] Xiao, F.; Chen, K.; Tong, Q. Magnetization textures in twisted bilayer CrX₃ (X=Br, I). *Phys. Rev. Res.* **2021**, *3*, 013027.
- [7] Akram, M.; LaBollita, H.; Dey, D.; Kapeghian, J.; Erten, O.; Botana, A. S. Moiré skyrmions and chiral magnetic phases in twisted CrX₃ (X= I, Br, and Cl) bilayers. *Nano Letters* **2021**, *21*, 6633–6639.
- [8] Zheng, F. Magnetic Skyrmion Lattices in a Novel 2D-Twisted Bilayer Magnet. *Advanced Functional Materials* **2023**, *33*, 2206923.
- [9] Li, Y. F.; Wang, W.; Guo, W.; Gu, C. Y.; Sun, H. Y.; He, L.; Zhou, J.; Gu, Z. B.; Nie, Y. F.; Pan, X. Q. Electronic structure of ferromagnetic semiconductor CrGeTe₃ by angle-resolved photoemission spectroscopy. *Phys. Rev. B* **2018**, *98*, 125127.
- [10] Webster, L.; Yan, J.-A. Strain-tunable magnetic anisotropy in monolayer CrCl₃, CrBr₃, and CrI₃. *Phys. Rev. B* **2018**, *98*, 144411.
- [11] Zheng, F.; Zhao, J.; Liu, Z.; Li, M.; Zhou, M.; Zhang, S.; Zhang, P. Tunable spin states in the two-dimensional magnet CrI₃. *Nanoscale* **2018**, *10*, 14298–14303.
- [12] Verzhbitskiy, I. A.; Kurebayashi, H.; Cheng, H.; Zhou, J.; Khan, S.; Feng, Y. P.; Eda, G. Controlling the magnetic anisotropy in Cr₂Ge₂Te₆ by electrostatic gating. *Nature Electronics* **2020**, *3*, 460–465.
- [13] Jiang, S.; Li, L.; Wang, Z.; Mak, K. F.; Shan, J. Controlling magnetism in 2D CrI₃ by electrostatic doping. *Nature Nanotechnology* **2018**, *13*, 549–553.
- [14] Zhang, W.-B.; Qu, Q.; Zhu, P.; Lam, C.-H. Robust intrinsic ferromagnetism and half semi-conductivity in stable two-dimensional single-layer chromium trihalides. *J. Mater. Chem. C*

- 2015**, *3*, 12457–12468.
- [15] Hou, Y.; Wei, Y.; Yang, D.; Wang, K.; Ren, K.; Zhang, G. Enhancing the Curie Temperature in $\text{Cr}_2\text{Ge}_2\text{Te}_6$ via Charge Doping: A First-Principles Study. *Molecules* **2023**, *28*, 3893
- [16] Deng, Y.; Yu, Y.; Song, Y.; Zhang, J.; Wang, N. Z.; Sun, Z.; Yi, Y.; Wu, Y. Z.; Wu, S.; Zhu, J.; Wang, J.; Chen, X. H.; Zhang, Y. Gate-tunable room-temperature ferromagnetism in two-dimensional Fe_3GeTe_2 . *Nature* **2018**, *563*, 94–99.
- [17] Fei, Z.; Huang, B.; Malinowski, P.; Wang, W.; Song, T.; Sanchez, J.; Yao, W.; Xiao, D.; Zhu, X.; May, A. F.; Wu, W.; Cobden, D. H.; Chu, J.-H.; Xu, X. Two-dimensional itinerant ferromagnetism in atomically thin Fe_3GeTe_2 . *Nature Materials* **2018**, *17*, 778–782.
- [18] Li, Z.; Xia, W.; Su, H.; Yu, Z.; Fu, Y.; Chen, L.; Wang, X.; Yu, N.; Zou, Z.; Guo, Y. Magnetic critical behavior of the van der Waals Fe_5GeTe_2 crystal with near room temperature ferromagnetism. *Scientific Reports* **2020**, *10*, 15345.
- [19] Bonilla, M.; Kolekar, S.; Ma, Y.; Diaz, H. C.; Kalappattil, V.; Das, R.; Eggers, T.; Gutierrez, H. R.; Phan, M.-H.; Batzill, M. Strong room-temperature ferromagnetism in VSe_2 monolayers on van der Waals substrates. *Nature Nanotechnology* **2018**, *13*, 289–293.
- [20] Lin, M.-W.; Zhuang, H. L.; Yan, J.; Ward, T. Z.; Puzniak, A. A.; Rouleau, C. M.; Gai, Z.; Liang, L.; Meunier, V.; Sumpter, B. G.; Ganesh, P.; Kent, P. R. C.; Geohegan, D. B.; Mandrus, D. G.; Xiao, K. Ultrathin nanosheets of CrSiTe_3 : a semiconducting two-dimensional ferromagnetic material. *J. Mater. Chem. C* **2016**, *4*, 315–322.
- [21] Zhang, G.; Guo, F.; Wu, H.; Wen, X.; Yang, L.; Jin, W.; Zhang, W.; Chang, H. Above-room-temperature strong intrinsic ferromagnetism in 2D van der Waals Fe_3GaTe_2 with large perpendicular magnetic anisotropy. *Nature Communications* **2022**, *13*, 5067.
- [22] Yin, H.; Zhang, P.; Jin, W.; Di, B.; Wu, H.; Zhang, G.; Zhang, W.; Chang, H. $\text{Fe}_3\text{GaTe}_2/\text{MoSe}_2$ ferromagnet/semiconductor 2D van der Waals heterojunction for room-temperature spin-valve devices. *CrystEngComm* **2023**, *25*, 1339–1346.
- [23] Jin, W.; Zhang, G.; Wu, H.; Yang, L.; Zhang, W.; Chang, H. Room-temperature spin-valve devices based on $\text{Fe}_3\text{GaTe}_2/\text{MoS}_2/\text{Fe}_3\text{GaTe}_2$ 2D van der Waals heterojunctions. *Nanoscale* **2023**, *15*, 5371–5378.
- [24] Jin, W.; Zhang, G.; Wu, H.; Yang, L.; Zhang, W.; Chang, H. Room-Temperature and Tunable Tunneling Magnetoresistance in Fe_3GaTe_2 -Based 2D van der Waals Heterojunctions. *ACS Applied Materials & Interfaces* **2023**, *15*, 36519–36526.

- [25] Wang, C. et al. Sign-tunable exchange bias effect in proton-intercalated Fe_3GaTe_2 nanoflakes. *Phys. Rev. B* **2023**, *107*, L140409.
- [26] Kresse, G.; Hafner, J. Ab initio molecular dynamics for liquid metals. *Phys. Rev. B* **1993**, *47*, 558–561.
- [27] Kresse, G.; Furthmüller, J. Efficient iterative schemes for ab initio total-energy calculations using a plane-wave basis set. *Phys. Rev. B* **1996**, *54*, 11169–11186.
- [28] Blöchl, P. E. Projector augmented-wave method. *Phys. Rev. B* **1994**, *50*, 17953–17979.
- [29] Perdew, J. P.; Burke, K.; Ernzerhof, M. Generalized Gradient Approximation Made Simple. *Phys. Rev. Lett.* **1996**, *77*, 3865–3868.
- [30] Togo, A.; Tanaka, I. First principles phonon calculations in materials science. *Scripta Materialia* **2015**, *108*, 1–5.
- [31] Metropolis, N.; Ulam, S. The Monte Carlo Method. *Journal of the American Statistical Association* **1949**, *44*, 335–341, PMID: 18139350.
- [32] Xiang, H. J.; Kan, E. J.; Wei, S.-H.; Whangbo, M.-H.; Gong, X. G. Predicting the spin-lattice order of frustrated systems from first principles. *Phys. Rev. B* **2011**, *84*, 224429.
- [33] Yu, M.; Trinkle, D. R. Accurate and efficient algorithm for Bader charge integration. *The Journal of Chemical Physics* **2011**, *134*, 064111.